Acta Cryst E CRYSTALLOGRAPHIC COMMUNICATIONS

ISSN 2056-9890

Crystal structure of bis{3-(3,4-dimethoxyphenyl)-5-[6-(pyrazol-1-yl)pyridin-2-yl]-1,2,4-triazol-3-ato}-iron(II)–methanol–chloroform (1/2/2)

Kateryna Znovjyak,[a] Igor O. Fritsky,[a] Tatiana Y. Sliva,[a] Vladimir M. Amirkhanov,[a] Sergey O. Malinkin,[a] Sergiu Shova[b] and Maksym Seredyuk[a]*

[a]Department of Chemistry, Taras Shevchenko National University of Kyiv, Volodymyrska Street 64, Kyiv, 01601, Ukraine, and [b]Department of Inorganic Polymers, "Petru Poni" Institute of Macromolecular, Chemistry, Romanian Academy of Science, Aleea Grigore Ghica Voda 41-A, Iasi, 700487, Romania. *Correspondence e-mail: mlseredyuk@gmail.com

Received 18 September 2023
Accepted 26 September 2023

Edited by B. Therrien, University of Neuchâtel, Switzerland

Keywords: crystal structure; iron(II) complexes; neutral complexes.

CCDC reference: 2297496

Supporting information: this article has supporting information at journals.iucr.org/e

The unit cell of the title compound, $[Fe(C_{18}H_{15}N_6O_2)_2]\cdot 2CH_3OH\cdot 2CHCl_3$, consists of a charge-neutral complex molecule, two methanol and two chloroform molecules. In the complex, the two tridentate 2-(5-(3,4-dimethoxyphenyl)-1,2,4-triazol-3-yl)-6-(pyrazol-1-yl)pyridine ligands coordinate to the central Fe^{II} ion through the N atoms of the pyrazole, pyridine and triazole groups, forming a pseudo-octahedral coordination sphere. Neighbouring tapered molecules are linked through weak C—H(pz)···π(ph) interactions into one-dimensional chains, which are joined into two-dimensional layers through weak C—H···N/C/O interactions. Furthermore, the layers stack in a three-dimensional network linked by weak interlayer C—H···π interactions of the methoxy and phenyl groups. The intermolecular contacts were quantified using Hirshfeld surface analysis and two-dimensional fingerprint plots, revealing the relative contributions of the contacts to the crystal packing to be H···H 32.0%, H···C/C···H 26.3%, H···N/N···H 13.8%, and H···O/O···H 7.5%. The average Fe—N bond distance is 2.185 Å, indicating the high-spin state of the Fe^{II} ion. Energy framework analysis at the HF/3–21 G theory level was performed to quantify the interaction energies in the crystal structure.

1. Chemical context

A broad class of coordination compounds exhibiting spin-state switching between low- (total spin S = 0) and high-spin states (total spin S = 2) is represented by Fe^{II} complexes based on tridentate bisazolepyridine ligands (Halcrow, 2014; Suryadevara *et al.*, 2022; Halcrow *et al.*, 2019). In the case of asymmetric ligand design, where one of the azole groups carries a hydrogen on a nitrogen heteroatom and acts as a Brønsted acid, deprotonation can produce neutral complexes that can be either high spin (Schäfer *et al.*, 2013) or low spin (Shiga *et al.*, 2019) or exhibit temperature-induced transition between the spin states of the central atom (Seredyuk *et al.*, 2014; Grunwald *et al.*, 2023) depending on the ligand field strength. The periphery of the molecule, *i.e.* ligand substituents, also plays an important role in the behaviour, determining the way that molecules are packed in the crystal and their interactions with each other, and therefore further influencing the spin state adopted by the central atom. For example, the dynamic rearrangement of the methoxy group between bent and extended configurations can lead to a highly hysteretic spin transition *via* a supramolecular blocking mechanism (Seredyuk *et al.*, 2022).

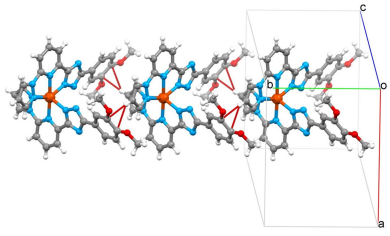

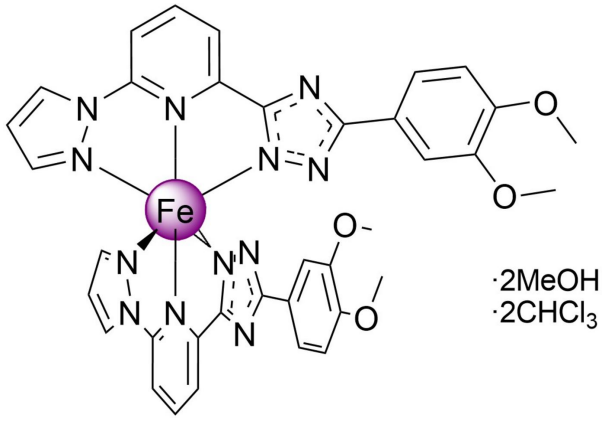

Having interest in spin-transition 3*d*-metal complexes formed by polydentate ligands (Bartual-Murgui *et al.*, 2017; Bonhommeau *et al.*, 2012; Valverde-Muñoz *et al.*, 2020), we report here a new $[Fe^{II}L_2]$ complex based on the asymmetric deprotonable ligand with two substituents on the phenyl group, *L* = 2-(5-(3,4-dimethoxyphenyl)-1,2,4-triazol-3-yl)-6-(pyrazol-1-yl)pyridine.

2. Structural commentary

The complex has a tapered structure with divergent phenyl groups. The ligand molecules are almost planar, including the methoxy substituents, which are also in the plane of the phenyl group. The independent methanol molecule forms O—H···N hydrogen bonds with the triazole (trz) rings of the ligand molecule (Fig. 1, Table 1). The chloroform molecules form double weak C—H···O bonds with the methoxy groups of the ligand. The central Fe^{II} ion of the complex has a distorted octahedral N_6 coordination environment formed by the nitrogen donor atoms of two tridentate ligands (Fig. 1). The average bond length, <Fe—N> = 2.185 Å, is typical for high-spin complexes with an N_6 coordination environment (Gütlich & Goodwin, 2004). The average trigonal distortion parameters $\Sigma = \Sigma_1^{12}(|90 - \varphi_i|)$, where φ_i is the angle N—Fe—N′ (Drew *et al.*, 1995), and $\Theta = \Sigma_1^{24}(|60 - \theta_i|)$, where θ_i is the angle generated by superposition of two opposite faces of an octahedron (Chang *et al.*, 1990) are 148.6 and 474.2°, respectively. The values reveal a deviation of the coordination environment from an ideal octahedron (where $\Sigma = \Theta = 0$), which is, however, in the expected range for bisazolepyridine and similar ligands (see below). The calculated continuous shape measure (CShM) value relative to the ideal O_h symmetry is 5.391 (Kershaw Cook *et al.*, 2015). The volume of the $[FeN_6]$ coordination polyhedron is 12.796 $Å^3$.

Table 1
Hydrogen-bond geometry (Å, °).

D—H···*A*	*D*—H	H···*A*	*D*···*A*	*D*—H···*A*
C2—H2···C14^{i}	0.95	2.85	3.676 (5)	146
C2—H2···C15^{i}	0.95	2.64	3.585 (5)	171
C7—H7···C1^{ii}	0.95	2.81	3.705 (5)	158
C1—H1···N6^{iii}	0.95	2.34	3.267 (5)	166
C12—H12···C9^{iv}	0.95	2.85	3.541 (5)	130
C20—H20···O1	1.00	2.28	3.115 (6)	141
C20—H20···O2	1.00	2.39	3.179 (6)	135
O3—H3*A*···N5	0.84	1.94	2.775 (4)	177
C3—H3···O3^{v}	0.95	2.33	3.238 (5)	161
C5—H5···O3^{v}	0.95	2.47	3.401 (6)	167

Symmetry codes: (i) $-x+1, y+1, -z+\frac{3}{2}$; (ii) $x+\frac{1}{2}, y-\frac{1}{2}, -z+\frac{3}{2}$; (iii) $x-\frac{1}{2}, y+\frac{1}{2}, -z+\frac{3}{2}$; (iv) $-x+\frac{3}{2}, y-\frac{1}{2}, z$; (v) $x+\frac{1}{2}, y+\frac{1}{2}, -z+\frac{3}{2}$.

3. Supramolecular features

Due to the tapered structure, neighbouring complex molecules fit into each other and interact through a weak C—H(pz)···π(ph) intermolecular contact between the pyrazole (pz) and phenyl (ph) groups respectively [the C2···*Cg*(ph) distance is 3.574 (5) Å]. The one-dimensional supramolecular chains formed extend along the *b*-axis direction with the stacking periodicity equal to 10.281 (3) Å (= cell parameter *b*) (Fig. 2). Through weak intermolecular C—H(pz, py)··· N/C(pz, trz) interactions in the range 3.115–3.705 (5) Å (Table 1), neighbouring chains are joined into corrugated two-dimensional layers in the *ab* plane (Fig. S1*a*,*b* in the supporting information). The layers stack without any interlayer interactions below the van der Waals radii (Fig. S1*b*

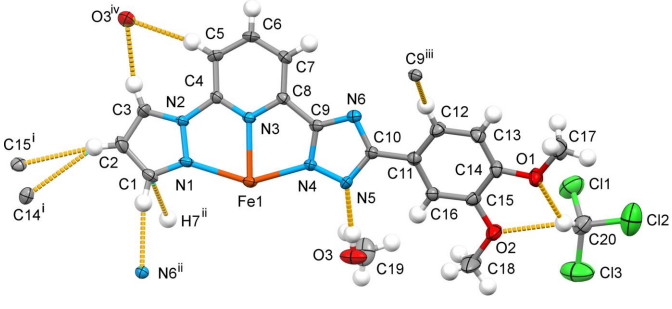

Figure 1
The molecular structure of a half of the title compound with displacement ellipsoids drawn at the 50% probability level. The strong O—H···N and weak C—H···O/N/C hydrogen bonds are shown with the nearest neighbours. Symmetry codes: (i) $1-x, 1+y, \frac{3}{2}-z$; (ii) $-\frac{1}{2}+x, \frac{1}{2}+y, \frac{3}{2}-z$; (iii) $\frac{3}{2}-x, -\frac{1}{2}+y, z$; (iv) $\frac{1}{2}+x, \frac{1}{2}+y, \frac{3}{2}-z$.

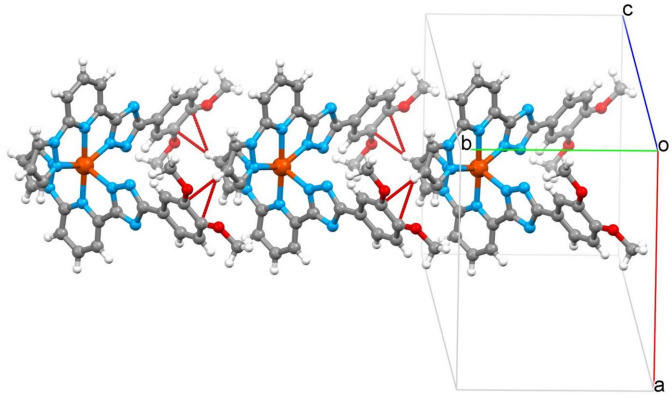

Figure 2
One-dimensional supramolecular chain formed by stacking molecules of the title compound. Red dashed lines correspond to contacts between the pyrazole and phenyl groups of neighbouring molecules below the sum of van der Waals radii.

in the supporting information). The voids between the layers are occupied by solvent molecules, which also participate in the bonding within separate layers. The methanol molecule forms a strong O—H···N hydrogen bond with the deprotonated triazole group, and a chloroform molecule located between two methoxy groups of the phenyl substituent forms a five-membered cyclic motif with two C—H···O bonds (see Fig. 1). A complete list of the considered intermolecular interactions is given in Table 1.

4. Hirshfeld surface and 2D fingerprint plots

Hirshfeld surface analysis was performed and the associated two-dimensional fingerprint plots were generated using *CrystalExplorer* (Spackman *et al.*, 2021), with a standard resolution of the three-dimensional d_{norm} surfaces plotted over a fixed colour scale of −0.6492 (red) to 1.3918 (blue) a.u. (Fig. 3*a*). The pale-red spots symbolize short contacts and negative d_{norm} values on the surface corresponding to the interactions described above. The overall two-dimensional fingerprint plot is illustrated in Fig. 4. The two-dimensional fingerprint plots, with their relative contributions to the Hirshfeld surface, are shown for the H···H, H···C/C···H, H···N/N···H and H···O/O···H contacts together with the . At 32.0%, the largest contribution to the overall crystal packing is from H···H interactions, which are located in the middle region of the fingerprint plot. H···C/C···H contacts contribute 26.3% to the Hirshfeld surface and result in a pair of characteristic wings. The H···N/N···H contacts, represented by a pair of sharp spikes in the fingerprint plot, make a 13.8% contribution to the Hirshfeld surface. Finally, H···O/O···H contacts, which account for a 7.5% contribution, are mostly distributed in the middle part of the plot. The electrostatic potential energy calculated using the HF/3-21G basis set localizes the negative charge on the trz-ph moieties of the complex molecule, while the pz-py moieties are relatively positively charged (Fig. 3*b*). The polar nature of the molecule justifies the stacking in columns.

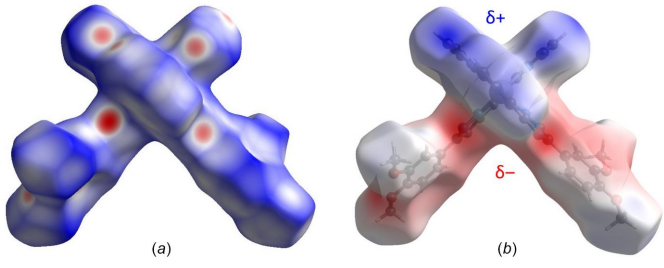

Figure 3
(*a*) A projection of d_{norm} mapped on the Hirshfeld surfaces, showing the intermolecular interactions within the molecule. Red/blue and white areas represent regions where contacts are shorter/larger than the sum and close to the sum of the van der Waals radii, respectively. (*b*) Electrostatic potential for the title compound derived from a HF/3–21 G wavefunction mapped on the Hirshfeld surface in the range −0.1658 (red) to 0.1235 a.u. (blue).

5. Energy framework analysis

The energy framework (Spackman *et al.*, 2021), calculated using the wave function at the HF/3-21G theory level, including the electrostatic potential forces (E_{ele}), the dispersion forces (E_{dis}) and the total energy diagrams (E_{tot}), is shown in Fig. S2 in the supporting information. The cylindrical radii, adjusted to the same scale factor of 100, are proportional to the relative strength of the corresponding energies. The major contribution is due to the dispersion forces (E_{dis}), reflecting dominating interactions in the crystal of the neutral asymmetric molecules. The topology of the energy framework resembles the topology of the interactions within and between the layers described above. The calculated value E_{tot} for the intrachain interaction is −57.2 kJ mol^{-1} and for interchain interactions are down to −114.6 kJ mol^{-1}. The interlayer interaction energies are close to zero. The colour-coded interaction mappings within a radius of 5.0 Å of a central reference molecule for the title compound together with full details of the various contributions to the total energy (E_{ele}, E_{pol}, E_{dis}, E_{rep}) are shown in the table in Figure S2.

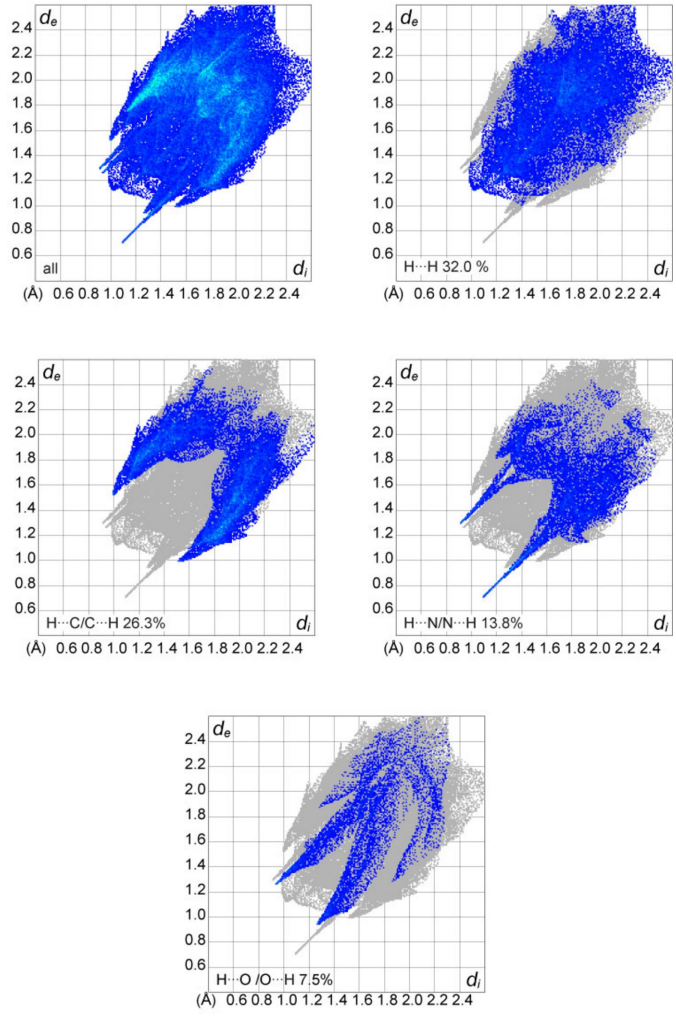

Figure 4
The overall two-dimensional fingerprint plot and those decomposed into specified interactions.

Table 2
Computed distortion indices (Å, °) for the title compound and for similar complexes reported in the literature.

CSD Code	Spin state	<Fe—N>	Σ	Θ	CShM(O_h)
Title compound	High-spin	2.185	148.6	474.2	5.39
IGERIX	High spin	2.179	149.7	553.2	6.06
IGERIX01	Low spin	1.986	105.6	350.6	2.85
LUTGEO	Low spin	1.933	85.0	309.6	2.10
XODCEB	Low spin	1.950	87.4	276.6	1.93
DOMQIH	Low spin	1.962	83.8	280.7	2.02
QIDJET01	Low spin	1.970	90.3	341.3	2.47
QIDJET	High spin	2.184	145.5	553.3	5.88
DOMQUT	Low spin	1.991	88.5	320.0	2.48
DOMQUT02	High spin	2.183	139.6	486.9	5.31
NIRLOT	Low spin	1.939	77.3	255.6	1.68

6. Database survey

A search of the Cambridge Structural Database (CSD, Version 5.42, last update February 2021; Groom *et al.*, 2016) reveals several similar neutral Fe^{II} complexes with a deprotonable azole group, for example, derivatives of a pyrazole-pyridinetetrazole, IGERIX and LUTGEO (Gentili *et al.*, 2015; Senthil Kumar *et al.*, 2015) and pyrazole-pyridine-benzimidazole XODCEB (Shiga *et al.*, 2019). In addition, there are related complexes based on phenathrolinetetrazole, such as QIDJET (Zhang *et al.*, 2007), phenanthroline-benzimidazole, DOMQUT (Seredyuk *et al.*, 2014), dipyridylpyrrol, NIRLOT (Grunwald *et al.*, 2023). The Fe—N distances of these complexes in the low-spin state are 1.933–1.959 Å, while in the high-spin state they are in the range 2.179–2.185 Å. The values of the trigonal distortion and CShM(O_h) change correspondingly, and in the low-spin state they are systematically lower than in the high-spin state. Table 2 collates the structural parameters of the complexes and of the title compound.

7. Synthesis and crystallization

The synthesis of the title compound is identical to that reported recently for a similar complex (Seredyuk *et al.*, 2022). It was produced by using a layering technique in a standard test tube. The layering sequence was as follows: the bottom layer contained a solution of $[Fe(L_2)](BF_4)_2$ prepared by dissolving L = 2-[5-(3,4-dimethoxyphenyl)-1,2,4-triazol-3-yl]-6-(pyrazol-1-yl)pyridine (88 mg, 0.252 mmol) and $Fe(BF_4)_2\cdot 6H_2O$ (43 mg, 0.126 mmol) in boiling acetone, to which chloroform (5 ml) was then added. The middle layer was a methanol–chloroform mixture (1:10, 10 ml), which was covered by a layer of methanol (10 ml), to which 100 ml of NEt_3 were added dropwise. The tube was sealed, and black–orange single crystals appeared after 3–4 weeks (yield *ca* 60%). Elemental analysis calculated for $C_{40}H_{40}Cl_6FeN_{12}O_6$: C, 45.61; H, 3.83; N, 15.96. Found: C, 45.52; H, 3.77; N, 15.77.

8. Refinement

Crystal data, data collection and structure refinement details are summarized in Table 3. H atoms were refined as riding [C—H = 0.95–0.98 Å with U_{iso}(H) = 1.2–1.5U_{eq}(C)]. The O-bound H atom was refined with U_{iso}(H) = 1.5U_{eq}(O).

Table 3
Experimental details.

Crystal data	
Chemical formula	$[Fe(C_{18}H_{15}N_6O_2)_2]\cdot 2CH_4O\cdot 2CHCl_3$
M_r	1053.39
Crystal system, space group	Orthorhombic, *Pbcn*
Temperature (K)	180
a, *b*, *c* (Å)	12.7195 (9), 10.281 (3), 36.735 (3)
V (Å^3)	4804.0 (13)
Z	4
Radiation type	Mo *Kα*
μ (mm^{-1})	0.71
Crystal size (mm)	0.25 × 0.2 × 0.03
Data collection	
Diffractometer	Xcalibur, Eos
Absorption correction	Multi-scan (*CrysAlis PRO*; Rigaku OD, 2022)
T_{min}, T_{max}	0.995, 1.000
No. of measured, independent and observed [$I > 2\sigma(I)$] reflections	18857, 5510, 2962
R_{int}	0.092
(sin $\theta/\lambda)_{max}$ (Å^{-1})	0.688
Refinement	
$R[F^2 > 2\sigma(F^2)]$, $wR(F^2)$, *S*	0.079, 0.145, 1.03
No. of reflections	5510
No. of parameters	298
H-atom treatment	H-atom parameters constrained
$\Delta\rho_{max}$, $\Delta\rho_{min}$ (e Å^{-3})	0.39, −0.44

Computer programs: *CrysAlis PRO* (Rigaku OD, 2022), *SHELXT* (Sheldrick, 2015*a*), *SHELXL2018/3* (Sheldrick, 2015*b*) and *OLEX2* (Dolomanov *et al.*, 2009).

Acknowledgements

Author contributions are as follows: Conceptualization, KZ and MS; methodology, KZ; formal analysis, IOF; synthesis, SOM; single-crystal measurements, SS; writing (original draft), MS; writing (review and editing of the manuscript), TYS, MS; visualization and calculations, KZ, VMA; funding acquisition, MS, IOF, VMA.

Funding information

Funding for this research was provided by a grant from the Ministry of Education and Science of Ukraine for perspective development of the scientific direction 'Mathematical sciences and natural sciences' at Taras Shevchenko National University of Kyiv and by the Ministry of Education and Science of Ukraine (grant Nos. 22BF037-03, 22BF037-04).

References

Bartual-Murgui, C., Piñeiro-López, L., Valverde-Muñoz, F. J., Muñoz, M. C., Seredyuk, M. & Real, J. A. (2017). *Inorg. Chem.* **56**, 13535–13546.
Bonhommeau, S., Lacroix, P. G., Talaga, D., Bousseksou, A., Seredyuk, M., Fritsky, I. O. & Rodriguez, V. (2012). *J. Phys. Chem. C*, **116**, 11251–11255.

Chang, H. R., McCusker, J. K., Toftlund, H., Wilson, S. R., Trautwein, A. X., Winkler, H. & Hendrickson, D. N. (1990). *J. Am. Chem. Soc.* **112**, 6814–6827.
Dolomanov, O. V., Bourhis, L. J., Gildea, R. J., Howard, J. A. K. & Puschmann, H. (2009). *J. Appl. Cryst.* **42**, 339–341.
Drew, M. G. B., Harding, C. J., McKee, V., Morgan, G. G. & Nelson, J. (1995). *J. Chem. Soc. Chem. Commun.* pp. 1035–1038.
Gentili, D., Demitri, N., Schäfer, B., Liscio, F., Bergenti, I., Ruani, G., Ruben, M. & Cavallini, M. (2015). *J. Mater. Chem. C.* **3**, 7836–7844.
Groom, C. R., Bruno, I. J., Lightfoot, M. P. & Ward, S. C. (2016). *Acta Cryst.* B**72**, 171–179.
Grunwald, J., Torres, J., Buchholz, A., Näther, C., Kämmerer, L., Gruber, M., Rohlf, S., Thakur, S., Wende, H., Plass, W., Kuch, W. & Tuczek, F. (2023). *Chem. Sci.* **14**, 7361–7380.
Gütlich, P. & Goodwin, H. A. (2004). *Top. Curr. Chem.* **233**, 1–47.
Halcrow, M. A. (2014). *New J. Chem.* **38**, 1868–1882.
Halcrow, M. A., Capel Berdiell, I., Pask, C. M. & Kulmaczewski, R. (2019). *Inorg. Chem.* **58**, 9811–9821.
Kershaw Cook, L. J., Mohammed, R., Sherborne, G., Roberts, T. D., Alvarez, S. & Halcrow, M. A. (2015). *Coord. Chem. Rev.* **289–290**, 2–12.
Rigaku OD (2022). *CrysAlis PRO*. Rigaku Oxford Diffraction, Yarnton, England.
Schäfer, B., Rajnák, C., Šalitroš, I., Fuhr, O., Klar, D., Schmitz-Antoniak, C., Weschke, E., Wende, H. & Ruben, M. (2013). *Chem. Commun.* **49**, 10986–10988.
Senthil Kumar, K., Šalitroš, I., Heinrich, B., Fuhr, O. & Ruben, M. (2015). *J. Mater. Chem. C.* **3**, 11635–11644.
Seredyuk, M., Znovjyak, K., Valverde-Muñoz, F. J., da Silva, I., Muñoz, M. C., Moroz, Y. S. & Real, J. A. (2022). *J. Am. Chem. Soc.* **144**, 14297–14309.
Seredyuk, M., Znovjyak, K. O., Kusz, J., Nowak, M., Muñoz, M. C. & Real, J. A. (2014). *Dalton Trans.* **43**, 16387–16394.
Sheldrick, G. M. (2015*a*). *Acta Cryst.* A**71**, 3–8.
Sheldrick, G. M. (2015*b*). *Acta Cryst.* C**71**, 3–8.
Shiga, T., Saiki, R., Akiyama, L., Kumai, R., Natke, D., Renz, F., Cameron, J. M., Newton, G. N. & Oshio, H. (2019). *Angew. Chem. Int. Ed.* **58**, 5658–5662.
Spackman, P. R., Turner, M. J., McKinnon, J. J., Wolff, S. K., Grimwood, D. J., Jayatilaka, D. & Spackman, M. A. (2021). *J. Appl. Cryst.* **54**, 1006–1011.
Suryadevara, N., Mizuno, A., Spieker, L., Salamon, S., Sleziona, S., Maas, A., Pollmann, E., Heinrich, B., Schleberger, M., Wende, H., Kuppusamy, S. K. & Ruben, M. (2022). *Chem. A Eur. J.* **28**, e202103853.
Valverde-Muñoz, F., Seredyuk, M., Muñoz, M. C., Molnár, G., Bibik, Y. S. & Real, J. A. (2020). *Angew. Chem. Int. Ed.* **59**, 18632–18638.
Zhang, W., Zhao, F., Liu, T., Yuan, M., Wang, Z. M. & Gao, S. (2007). *Inorg. Chem.* **46**, 2541–2555.

supporting information

Acta Cryst. (2023). E**79**, 962-966 [https://doi.org/10.1107/S2056989023008423]

Crystal structure of bis{3-(3,4-dimethoxyphenyl)-5-[6-(pyrazol-1-yl)pyridin-2-yl]-1,2,4-triazol-3-ato}iron(II)–methanol–chloroform (1/2/2)

Kateryna Znovjyak, Igor O. Fritsky, Tatiana Y. Sliva, Vladimir M. Amirkhanov, Sergey O. Malinkin, Sergiu Shova and Maksym Seredyuk

Computing details

Data collection: *CrysAlis PRO* 1.171.41.123a (Rigaku OD, 2022); cell refinement: *CrysAlis PRO* 1.171.41.123a (Rigaku OD, 2022); data reduction: *CrysAlis PRO* 1.171.41.123a (Rigaku OD, 2022); program(s) used to solve structure: *SHELXT* (Sheldrick, 2015a); program(s) used to refine structure: *SHELXL2018/3* (Sheldrick, 2015b); molecular graphics: Olex2 1.3 (Dolomanov *et al.*, 2009); software used to prepare material for publication: Olex2 1.3 (Dolomanov *et al.*, 2009).

Bis{3-(3,4-dimethoxyphenyl)-5-[6-(pyrazol-1-yl)pyridin-2-yl]-\ 1,2,4-triazol-3-ato}iron(II)–methanol–chloroform (1/2/2)

Crystal data

$[Fe(C_{18}H_{15}N_6O_2)_2]\cdot 2CH_4O\cdot 2CHCl_3$
$M_r = 1053.39$
Orthorhombic, *Pbcn*
$a = 12.7195$ (9) Å
$b = 10.281$ (3) Å
$c = 36.735$ (3) Å
$V = 4804.0$ (13) Å^3
$Z = 4$
$F(000) = 2160$
$D_x = 1.456$ Mg m^{-3}
Mo $K\alpha$ radiation, $\lambda = 0.71073$ Å
Cell parameters from 2694 reflections
$\theta = 2.0$–$22.1°$
$\mu = 0.71$ mm^{-1}
$T = 180$ K
Prism, clear light yellow
0.25 × 0.2 × 0.03 mm

Data collection

Xcalibur, Eos diffractometer
Radiation source: fine-focus sealed X-ray tube, Enhance (Mo) X-ray Source
Graphite monochromator
Detector resolution: 16.1593 pixels mm^{-1}
ω scans
Absorption correction: multi-scan (CrysAlisPro; Rigaku OD, 2022)
$T_{min} = 0.995$, $T_{max} = 1.000$
18857 measured reflections
5510 independent reflections
2962 reflections with $I > 2\sigma(I)$
$R_{int} = 0.092$
$\theta_{max} = 29.3°$, $\theta_{min} = 2.0°$
$h = -17\rightarrow14$
$k = -11\rightarrow13$
$l = -30\rightarrow45$

Refinement

Refinement on F^2
Least-squares matrix: full
$R[F^2 > 2\sigma(F^2)] = 0.079$
$wR(F^2) = 0.145$
$S = 1.03$
5510 reflections
298 parameters
0 restraints
Hydrogen site location: inferred from neighbouring sites

H-atom parameters constrained
$w = 1/[\sigma^2(F_o^2) + (0.0352P)^2 + 1.3579P]$
where $P = (F_o^2 + 2F_c^2)/3$

$(\Delta/\sigma)_{max} < 0.001$
$\Delta\rho_{max} = 0.39$ e Å^{-3}
$\Delta\rho_{min} = -0.44$ e Å^{-3}

Special details

Geometry. All esds (except the esd in the dihedral angle between two l.s. planes) are estimated using the full covariance matrix. The cell esds are taken into account individually in the estimation of esds in distances, angles and torsion angles; correlations between esds in cell parameters are only used when they are defined by crystal symmetry. An approximate (isotropic) treatment of cell esds is used for estimating esds involving l.s. planes.

Fractional atomic coordinates and isotropic or equivalent isotropic displacement parameters (Å^2)

	x	*y*	*z*	U_{iso}*/U_{eq}
Fe1	0.500000	0.76448 (9)	0.750000	0.0222 (2)
Cl1	0.66889 (10)	0.30702 (16)	0.48491 (4)	0.0718 (5)
Cl3	0.45098 (10)	0.2575 (2)	0.46990 (4)	0.0951 (7)
Cl2	0.60243 (13)	0.05279 (18)	0.46193 (4)	0.0862 (6)
N3	0.6647 (2)	0.7695 (3)	0.76381 (8)	0.0212 (8)
O1	0.6486 (2)	0.1131 (3)	0.56399 (8)	0.0363 (8)
N4	0.5728 (2)	0.6285 (3)	0.71371 (8)	0.0221 (8)
N2	0.6252 (2)	0.9304 (3)	0.80493 (9)	0.0236 (8)
N5	0.5447 (2)	0.5444 (3)	0.68666 (8)	0.0223 (8)
O2	0.4939 (2)	0.2752 (3)	0.56650 (8)	0.0427 (9)
N1	0.5214 (2)	0.9131 (3)	0.79464 (9)	0.0246 (8)
O3	0.3669 (2)	0.6194 (4)	0.64823 (9)	0.0525 (10)
H3A	0.421091	0.594475	0.659283	0.079*
N6	0.7165 (2)	0.5103 (3)	0.69940 (8)	0.0221 (8)
C9	0.6755 (3)	0.6051 (4)	0.72010 (10)	0.0216 (10)
C8	0.7306 (3)	0.6878 (4)	0.74638 (10)	0.0208 (9)
C14	0.6502 (3)	0.1976 (4)	0.59249 (11)	0.0272 (10)
C4	0.7027 (3)	0.8539 (4)	0.78750 (10)	0.0222 (10)
C16	0.5594 (3)	0.3751 (4)	0.62214 (11)	0.0261 (10)
H16	0.501808	0.433833	0.623005	0.031*
C3	0.6331 (3)	1.0150 (4)	0.83276 (12)	0.0348 (12)
H3	0.696474	1.042065	0.844178	0.042*
C12	0.7199 (3)	0.2910 (4)	0.64749 (11)	0.0296 (11)
H12	0.773273	0.291996	0.665593	0.036*
C7	0.8379 (3)	0.6927 (4)	0.75259 (11)	0.0295 (11)
H7	0.884266	0.634916	0.740344	0.035*
C10	0.6324 (3)	0.4768 (4)	0.67851 (10)	0.0222 (10)
C5	0.8097 (3)	0.8673 (4)	0.79519 (11)	0.0300 (11)
H5	0.835528	0.930144	0.811906	0.036*
C1	0.4682 (3)	0.9884 (4)	0.81718 (11)	0.0281 (11)
H1	0.393795	0.996704	0.816911	0.034*
C13	0.7257 (3)	0.2015 (4)	0.61954 (11)	0.0304 (11)
H13	0.782566	0.141665	0.618878	0.036*
C11	0.6377 (3)	0.3795 (4)	0.64968 (10)	0.0246 (10)
C2	0.5343 (3)	1.0548 (5)	0.84167 (13)	0.0399 (13)
H2	0.514382	1.114171	0.860259	0.048*

C15	0.5664 (3)	0.2858 (4)	0.59409 (11)	0.0266 (10)
C6	0.8757 (3)	0.7825 (5)	0.77677 (12)	0.0361 (12)
H6	0.949305	0.786965	0.781044	0.043*
C20	0.5675 (3)	0.1923 (5)	0.48712 (13)	0.0490 (14)
H20	0.556297	0.166973	0.513117	0.059*
C17	0.7283 (3)	0.0157 (5)	0.56289 (13)	0.0488 (14)
H17A	0.720138	−0.036527	0.540761	0.073*
H17B	0.721896	−0.040564	0.584307	0.073*
H17C	0.797583	0.057357	0.562860	0.073*
C19	0.3952 (4)	0.7063 (6)	0.62079 (14)	0.0644 (17)
H19A	0.433569	0.659748	0.601683	0.097*
H19B	0.440099	0.774643	0.630986	0.097*
H19C	0.331711	0.745638	0.610407	0.097*
C18	0.4062 (4)	0.3632 (6)	0.56791 (15)	0.085 (2)
H18A	0.357693	0.343789	0.547915	0.127*
H18B	0.431588	0.452834	0.565572	0.127*
H18C	0.369588	0.353055	0.591206	0.127*

Atomic displacement parameters (Å²)

	U^{11}	U^{22}	U^{33}	U^{12}	U^{13}	U^{23}
Fe1	0.0131 (4)	0.0258 (5)	0.0278 (4)	0.000	−0.0003 (3)	0.000
Cl1	0.0667 (9)	0.0745 (13)	0.0741 (11)	−0.0242 (8)	−0.0098 (7)	−0.0051 (10)
Cl3	0.0540 (9)	0.1473 (19)	0.0841 (12)	0.0051 (10)	−0.0120 (7)	0.0380 (14)
Cl2	0.1297 (13)	0.0655 (12)	0.0634 (11)	−0.0138 (11)	0.0108 (9)	−0.0116 (11)
N3	0.0149 (15)	0.023 (2)	0.0261 (18)	0.0011 (15)	−0.0012 (13)	−0.0012 (18)
O1	0.0454 (17)	0.029 (2)	0.0346 (18)	0.0121 (16)	−0.0062 (14)	−0.0080 (17)
N4	0.0150 (15)	0.026 (2)	0.0250 (19)	−0.0001 (15)	0.0003 (13)	−0.0049 (18)
N2	0.0133 (15)	0.023 (2)	0.034 (2)	0.0000 (14)	0.0004 (14)	−0.0089 (19)
N5	0.0204 (16)	0.024 (2)	0.0228 (18)	−0.0025 (15)	−0.0025 (13)	−0.0074 (18)
O2	0.0406 (17)	0.044 (2)	0.0439 (18)	0.0137 (16)	−0.0179 (14)	−0.0162 (18)
N1	0.0110 (15)	0.027 (2)	0.036 (2)	−0.0004 (14)	−0.0007 (13)	−0.0012 (19)
O3	0.0282 (15)	0.074 (3)	0.056 (2)	−0.0040 (18)	−0.0061 (15)	0.027 (2)
N6	0.0194 (16)	0.024 (2)	0.0232 (19)	−0.0008 (15)	−0.0015 (13)	0.0019 (17)
C9	0.0167 (19)	0.026 (3)	0.022 (2)	−0.0009 (18)	−0.0007 (15)	0.002 (2)
C8	0.0186 (19)	0.019 (2)	0.024 (2)	0.0022 (17)	0.0017 (16)	0.000 (2)
C14	0.035 (2)	0.022 (3)	0.025 (2)	0.004 (2)	0.0003 (18)	−0.001 (2)
C4	0.0177 (19)	0.023 (3)	0.026 (2)	−0.0007 (18)	0.0036 (16)	−0.003 (2)
C16	0.022 (2)	0.020 (3)	0.036 (3)	0.0009 (18)	−0.0020 (17)	−0.004 (2)
C3	0.024 (2)	0.034 (3)	0.046 (3)	−0.004 (2)	−0.0011 (19)	−0.019 (3)
C12	0.031 (2)	0.028 (3)	0.030 (2)	0.003 (2)	−0.0083 (18)	−0.001 (2)
C7	0.019 (2)	0.034 (3)	0.035 (2)	0.0060 (18)	0.0008 (17)	−0.010 (3)
C10	0.0180 (19)	0.023 (3)	0.025 (2)	−0.0001 (18)	0.0001 (16)	−0.002 (2)
C5	0.0190 (19)	0.034 (3)	0.037 (3)	−0.006 (2)	−0.0029 (18)	−0.008 (2)
C1	0.0181 (19)	0.026 (3)	0.040 (3)	0.0038 (18)	0.0061 (18)	0.000 (2)
C13	0.032 (2)	0.026 (3)	0.033 (3)	0.008 (2)	−0.0017 (18)	0.000 (2)
C11	0.024 (2)	0.024 (3)	0.025 (2)	−0.0024 (19)	0.0018 (17)	0.000 (2)
C2	0.032 (2)	0.035 (3)	0.053 (3)	0.006 (2)	0.009 (2)	−0.020 (3)

C15	0.026 (2)	0.023 (3)	0.031 (2)	−0.0042 (19)	−0.0047 (17)	−0.002 (2)
C6	0.0129 (19)	0.051 (4)	0.045 (3)	0.000 (2)	−0.0015 (18)	−0.011 (3)
C20	0.052 (3)	0.054 (4)	0.041 (3)	−0.008 (3)	−0.005 (2)	−0.002 (3)
C17	0.060 (3)	0.036 (3)	0.051 (3)	0.014 (3)	−0.003 (2)	−0.017 (3)
C19	0.096 (4)	0.051 (4)	0.047 (3)	0.007 (3)	0.001 (3)	0.013 (4)
C18	0.061 (3)	0.100 (6)	0.094 (5)	0.049 (4)	−0.051 (3)	−0.051 (5)

Geometric parameters (Å, º)

Fe1—N3	2.156 (3)	C4—C5	1.398 (5)
Fe1—N3^{i}	2.156 (3)	C16—H16	0.9500
Fe1—N4^{i}	2.142 (3)	C16—C11	1.420 (5)
Fe1—N4	2.142 (3)	C16—C15	1.383 (5)
Fe1—N1	2.258 (3)	C3—H3	0.9500
Fe1—N1^{i}	2.258 (3)	C3—C2	1.363 (5)
Cl1—C20	1.749 (5)	C12—H12	0.9500
Cl3—C20	1.745 (5)	C12—C13	1.380 (5)
Cl2—C20	1.764 (5)	C12—C11	1.389 (5)
N3—C8	1.348 (4)	C7—H7	0.9500
N3—C4	1.320 (5)	C7—C6	1.369 (5)
O1—C14	1.361 (5)	C10—C11	1.458 (5)
O1—C17	1.425 (5)	C5—H5	0.9500
N4—N5	1.365 (4)	C5—C6	1.386 (5)
N4—C9	1.349 (4)	C1—H1	0.9500
N2—N1	1.385 (4)	C1—C2	1.408 (6)
N2—C4	1.414 (4)	C13—H13	0.9500
N2—C3	1.346 (5)	C2—H2	0.9500
N5—C10	1.347 (4)	C6—H6	0.9500
O2—C15	1.374 (4)	C20—H20	1.0000
O2—C18	1.437 (5)	C17—H17A	0.9800
N1—C1	1.320 (5)	C17—H17B	0.9800
O3—H3A	0.8400	C17—H17C	0.9800
O3—C19	1.394 (5)	C19—H19A	0.9800
N6—C9	1.342 (5)	C19—H19B	0.9800
N6—C10	1.362 (4)	C19—H19C	0.9800
C9—C8	1.465 (5)	C18—H18A	0.9800
C8—C7	1.385 (5)	C18—H18B	0.9800
C14—C13	1.382 (5)	C18—H18C	0.9800
C14—C15	1.401 (5)		
N3^{i}—Fe1—N3	177.28 (19)	C11—C12—H12	119.3
N3—Fe1—N1	72.28 (11)	C8—C7—H7	120.7
N3^{i}—Fe1—N1	105.79 (11)	C6—C7—C8	118.5 (4)
N3^{i}—Fe1—N1^{i}	72.29 (11)	C6—C7—H7	120.7
N3—Fe1—N1^{i}	105.79 (11)	N5—C10—N6	113.2 (4)
N4^{i}—Fe1—N3	106.79 (11)	N5—C10—C11	123.6 (3)
N4—Fe1—N3^{i}	106.79 (11)	N6—C10—C11	123.1 (3)
N4^{i}—Fe1—N3^{i}	75.05 (12)	C4—C5—H5	122.3

N4—Fe1—N3	75.05 (12)	C6—C5—C4	115.4 (4)
N4—Fe1—N4^{i}	98.53 (18)	C6—C5—H5	122.3
N4^{i}—Fe1—N1^{i}	147.30 (10)	N1—C1—H1	123.9
N4^{i}—Fe1—N1	92.40 (12)	N1—C1—C2	112.3 (3)
N4—Fe1—N1	147.30 (10)	C2—C1—H1	123.9
N4—Fe1—N1^{i}	92.40 (12)	C14—C13—H13	119.4
N1—Fe1—N1^{i}	94.81 (17)	C12—C13—C14	121.2 (4)
C8—N3—Fe1	118.5 (3)	C12—C13—H13	119.4
C4—N3—Fe1	121.7 (2)	C16—C11—C10	120.5 (4)
C4—N3—C8	119.7 (3)	C12—C11—C16	117.8 (4)
C14—O1—C17	117.3 (3)	C12—C11—C10	121.7 (3)
N5—N4—Fe1	138.9 (2)	C3—C2—C1	104.6 (4)
C9—N4—Fe1	115.3 (3)	C3—C2—H2	127.7
C9—N4—N5	105.5 (3)	C1—C2—H2	127.7
N1—N2—C4	118.0 (3)	O2—C15—C14	115.3 (4)
C3—N2—N1	111.2 (3)	O2—C15—C16	124.0 (4)
C3—N2—C4	130.7 (3)	C16—C15—C14	120.6 (4)
C10—N5—N4	105.8 (3)	C7—C6—C5	121.9 (3)
C15—O2—C18	116.3 (3)	C7—C6—H6	119.1
N2—N1—Fe1	113.6 (2)	C5—C6—H6	119.1
C1—N1—Fe1	142.2 (2)	Cl1—C20—Cl2	109.8 (2)
C1—N1—N2	104.0 (3)	Cl1—C20—H20	109.0
C19—O3—H3A	109.5	Cl3—C20—Cl1	110.5 (3)
C9—N6—C10	101.4 (3)	Cl3—C20—Cl2	109.6 (3)
N4—C9—C8	118.3 (3)	Cl3—C20—H20	109.0
N6—C9—N4	114.1 (3)	Cl2—C20—H20	109.0
N6—C9—C8	127.5 (3)	O1—C17—H17A	109.5
N3—C8—C9	112.1 (3)	O1—C17—H17B	109.5
N3—C8—C7	120.8 (4)	O1—C17—H17C	109.5
C7—C8—C9	127.0 (4)	H17A—C17—H17B	109.5
O1—C14—C13	125.6 (4)	H17A—C17—H17C	109.5
O1—C14—C15	115.7 (3)	H17B—C17—H17C	109.5
C13—C14—C15	118.7 (4)	O3—C19—H19A	109.5
N3—C4—N2	114.2 (3)	O3—C19—H19B	109.5
N3—C4—C5	123.6 (4)	O3—C19—H19C	109.5
C5—C4—N2	122.2 (4)	H19A—C19—H19B	109.5
C11—C16—H16	119.8	H19A—C19—H19C	109.5
C15—C16—H16	119.8	H19B—C19—H19C	109.5
C15—C16—C11	120.5 (4)	O2—C18—H18A	109.5
N2—C3—H3	126.0	O2—C18—H18B	109.5
N2—C3—C2	107.9 (4)	O2—C18—H18C	109.5
C2—C3—H3	126.0	H18A—C18—H18B	109.5
C13—C12—H12	119.3	H18A—C18—H18C	109.5
C13—C12—C11	121.3 (4)	H18B—C18—H18C	109.5
Fe1—N3—C8—C9	−0.6 (4)	C9—N6—C10—N5	−1.6 (4)
Fe1—N3—C8—C7	175.9 (3)	C9—N6—C10—C11	177.0 (4)
Fe1—N3—C4—N2	5.5 (5)	C9—C8—C7—C6	175.8 (4)

Fe1—N3—C4—C5	−174.9 (3)	C8—N3—C4—N2	−177.7 (3)
Fe1—N4—N5—C10	−172.7 (3)	C8—N3—C4—C5	1.9 (6)
Fe1—N4—C9—N6	173.7 (3)	C8—C7—C6—C5	0.5 (7)
Fe1—N4—C9—C8	−9.8 (4)	C4—N3—C8—C9	−177.6 (3)
Fe1—N1—C1—C2	175.1 (3)	C4—N3—C8—C7	−1.0 (6)
N3—C8—C7—C6	−0.2 (6)	C4—N2—N1—Fe1	−1.3 (4)
N3—C4—C5—C6	−1.6 (6)	C4—N2—N1—C1	175.1 (3)
O1—C14—C13—C12	−179.6 (4)	C4—N2—C3—C2	−174.5 (4)
O1—C14—C15—O2	−0.2 (5)	C4—C5—C6—C7	0.3 (7)
O1—C14—C15—C16	179.2 (4)	C3—N2—N1—Fe1	−176.9 (3)
N4—N5—C10—N6	1.2 (4)	C3—N2—N1—C1	−0.5 (4)
N4—N5—C10—C11	−177.4 (3)	C3—N2—C4—N3	172.2 (4)
N4—C9—C8—N3	6.9 (5)	C3—N2—C4—C5	−7.4 (7)
N4—C9—C8—C7	−169.4 (4)	C10—N6—C9—N4	1.4 (4)
N2—N1—C1—C2	0.4 (5)	C10—N6—C9—C8	−174.7 (4)
N2—C4—C5—C6	178.0 (4)	C13—C14—C15—O2	−179.3 (4)
N2—C3—C2—C1	−0.2 (5)	C13—C14—C15—C16	0.1 (6)
N5—N4—C9—N6	−0.8 (4)	C13—C12—C11—C16	0.0 (6)
N5—N4—C9—C8	175.8 (3)	C13—C12—C11—C10	−178.2 (4)
N5—C10—C11—C16	17.2 (6)	C11—C16—C15—O2	179.9 (4)
N5—C10—C11—C12	−164.6 (4)	C11—C16—C15—C14	0.5 (6)
N1—N2—C4—N3	−2.5 (5)	C11—C12—C13—C14	0.6 (6)
N1—N2—C4—C5	177.9 (4)	C15—C14—C13—C12	−0.6 (6)
N1—N2—C3—C2	0.4 (5)	C15—C16—C11—C12	−0.6 (6)
N1—C1—C2—C3	−0.2 (5)	C15—C16—C11—C10	177.7 (4)
N6—C9—C8—N3	−177.1 (4)	C17—O1—C14—C13	3.5 (6)
N6—C9—C8—C7	6.6 (7)	C17—O1—C14—C15	−175.5 (4)
N6—C10—C11—C16	−161.3 (4)	C18—O2—C15—C14	179.0 (4)
N6—C10—C11—C12	16.9 (6)	C18—O2—C15—C16	−0.4 (6)
C9—N4—N5—C10	−0.3 (4)		

Symmetry code: (i) −*x*+1, *y*, −*z*+3/2.

Hydrogen-bond geometry (Å, º)

D—H···*A*	*D*—H	H···*A*	*D*···*A*	*D*—H···*A*
C2—H2···C14^{ii}	0.95	2.85	3.676 (5)	146
C2—H2···C15^{ii}	0.95	2.64	3.585 (5)	171
C7—H7···C1^{iii}	0.95	2.81	3.705 (5)	158
C1—H1···N6^{iv}	0.95	2.34	3.267 (5)	166
C12—H12···C9^{v}	0.95	2.85	3.541 (5)	130
C20—H20···O1	1.00	2.28	3.115 (6)	141
C20—H20···O2	1.00	2.39	3.179 (6)	135
O3—H3*A*···N5	0.84	1.94	2.775 (4)	177
C3—H3···O3^{vi}	0.95	2.33	3.238 (5)	161
C5—H5···O3^{vi}	0.95	2.47	3.401 (6)	167

Symmetry codes: (ii) −*x*+1, *y*+1, −*z*+3/2; (iii) *x*+1/2, *y*−1/2, −*z*+3/2; (iv) *x*−1/2, *y*+1/2, −*z*+3/2; (v) −*x*+3/2, *y*−1/2, *z*; (vi) *x*+1/2, *y*+1/2, −*z*+3/2.